AGU PUBLICATIONS

Geochemistry, Geophysics, Geosystems

RESEARCH ARTICLE

10.1002/2016GC006683

Contrasted hydrothermal activity along the South-East Indian Ridge (130°E–140°E): From crustal to ultramafic circulation

Cédric Boulart[1], Anne Briais[2], Valérie Chavagnac[2], Sidonie Révillon[3], Georges Ceuleneer[2], Jean-Pierre Donval[1], Vivien Guyader[1], Fabienne Barrere[2], Nicolas Ferreira[4], Barry Hanan[5], Christophe Hémond[4], Sarah Macleod[6], Marcia Maia[4], Agnès Maillard[2], Sergey Merkuryev[7], Sung-Hyun Park[8], Etienne Ruellan[2], Alexandre Schohn[4], Sally Watson[9], and Yun-Seok Yang[8]

[1]IFREMER, Géosciences Marines, Plouzané, France, [2]Géosciences Environnement Toulouse, UMR5563 CNRS/UPS/IRD/CNES, Toulouse, France, [3]Sedisor - Laboratoire Domaines Océaniques, IUEM, Brest, France, [4]CNRS, Domaines Océaniques, Institut Univ. Européen de la Mer, Plouzané, France, [5]Department of Geological Sciences, San Diego State University, San Diego, California, USA, [6]School of Geological Sciences, University of Sydney, Sydney, New South Wales, Australia, [7]IZMIRAN, St Petersburg, Russia, [8]Korea Polar Research Institute, Incheon, South Korea, [9]IMAS, University of Tasmania, Hobart, Tasmania, Australia

Key Points:
- Intense and contrasted hydrothermal activity has been evidenced along the South-East Indian Ridge in the Furious Fifties
- Ultramafic circulation is evidenced in the George V FZ, which is the first observation of this type along an intermediate-spreading ridge
- Chemical compositions of the plumes reveal various regional and local controls on the hydrothermal circulation

Supporting Information:
- Supporting Information S1

Correspondence to:
C. Boulart,
cedric.boulart@ifremer.fr

Citation:
Boulart, C., et al. (2017), Contrasted hydrothermal activity along the South-East Indian Ridge (130°E–140°E): From crustal to ultramafic circulation, *Geochem. Geophys. Geosyst.*, *18*, 2446–2458, doi:10.1002/2016GC006683.

Received 17 OCT 2016
Accepted 17 MAY 2017
Accepted article online 30 MAY 2017
Published online 3 JUL 2017

The last 13 authors belong to the STORM Cruise Science Party.

Abstract Using a combined approach of seafloor mapping, MAPR and CTD survey, we report evidence for active hydrothermal venting along the 130°-140°E section of the poorly-known South-East Indian Ridge (SEIR) from the Australia-Antarctic Discordance (AAD) to the George V Fracture Zone (FZ). Along the latter, we report Eh and CH_4 anomalies in the water column above a serpentinite massif, which unambiguously testify for ultramafic-related fluid flow. This is the first time that such circulation is observed on an intermediate-spreading ridge. The ridge axis itself is characterized by numerous off-axis volcanoes, suggesting a high magma supply. The water column survey indicates the presence of at least ten distinct hydrothermal plumes along the axis. The CH_4:Mn ratios of the plumes vary from 0.37 to 0.65 denoting different underlying processes, from typical basalt-hosted to ultramafic-hosted high-temperature hydrothermal circulation. Our data suggest that the change of mantle temperature along the SEIR not only regulates the magma supply, but also the hydrothermal activity. The distribution of hydrothermal plumes from a ridge segment to another implies secondary controls such as the presence of fractures and faults along the axis or in the axial discontinuities. We conclude from these results that hydrothermal activity along the SEIR is controlled by magmatic processes at the regional scale and by the tectonics at the segment scale, which influences the type of hydrothermal circulation and leads to various chemical compositions. Such variety may impact global biogeochemical cycles, especially in the Southern Ocean where hydrothermal venting might be the only source of nutrients.

1. Introduction

Deep-sea hydrothermal venting is a global-scale process, which occurs wherever fluid circulates in the oceanic crust close to a heat source, especially along mid-ocean ridges (MOR). This process enables the exchanges of heat and matter between the Earth's interior and the hydrosphere and modifies the chemistry of the ocean on the short and long timespans [*Edmond et al*., 1979; *Elderfield and Schultz*, 1996; *German and Seyfried*, 2014]. The knowledge on the distribution of hydrothermal vents across the global ridge network is therefore a key to the understanding and a more precise estimation of the chemical transfers to the ocean.

Hydrothermal plumes associated with physical and chemical anomalies in the water column are a well-known tool to locate high-temperature vents along MORs. At the global scale, the vent distribution is strongly correlated to the spreading rate, the latter being seen as a proxy for the long-term magmatic budget [*Baker and German*, 2004; *Baker et al*., 2014; *Son et al*., 2014]. Indeed, magmatic processes are predominant in the control of high-temperature venting, which requires continuous refill of magma lenses and is expressed, in terms of ridge morphology, as inflated axial cross sections with magma lenses close to the surface [*Baker et al*., 2014; *Son et al*., 2014]. Recent work [*Beaulieu et al*., 2015; *German et al*., 2016a] showed that this linear relationship is also valid for slow to ultraslow-spreading ridges, although hydrothermal venting is still observed at spreading rates close to zero. In fact, Deep Sea exploration along MORs revealed plume

activity away from magma chambers, which has been attributed to tectonically-induced fluid circulation below the seafloor, possibly fuelled by the reaction of water with ultramafics [*German et al*., 2016a]. This is especially true on slow to ultraslow-spreading ridges, where many ultramafic-hosted vents have been observed [*Charlou et al*., 2010; *Pedersen et al*., 2010; *Tao et al*., 2011]. But previous exploration revealed the presence of serpentinized peridotite outcrops in many places and geological features such as the St. Paul FZ on the slow-spreading Mid-Atlantic ridge [*Hekinian et al*., 2000; *Maia et al*., 2016] or the Garrett FZ on the fast-spreading East Pacific Rise [*Hekinian et al*., 1992], an observation which expands the possibility of finding ultramafic-related fluid flow on the global ridge-crest.

Based on the "spreading rate" model defined by *Baker et al*. [1995], *Beaulieu et al*. [2015] noted that about ~800 vent sites are still to be discovered along MORs, half of them on intermediate to fast-spreading ridges. To date, most of the 12,500 km-long, intermediate-spreading South East Indian Ridge (SEIR) between the Rodriguez and the Macquarie Triple Junctions in the southern hemisphere remains un-surveyed for hydrothermal activity [*Beaulieu et al*., 2015]. Thorough exploration has been carried out mainly along a 2,500 km section around the St. Paul-Amsterdam Plateau and to its east, from 77°E to 99°E [*Scheirer et al*., 1998; *Johnson et al*., 2000; *Baker et al*., 2014], and on the south-easternmost segments (152–161°E) where a hydrothermal vent was discovered [*Hahm et al*., 2015].

One important feature of the SEIR is the presence of the Australia-Antarctic Discordance (AAD) between 120°E and 128°E, an area of anomalous low magmatic budget with a typical ridge morphology of slow-spreading ridge despite an intermediate spreading rate of 75 mm/yr [*Weissel and Hayes*, 1974]. West of the AAD between 77 and 99°E, where the ridge axis has a dome-like morphology, *Baker et al*. [2014] showed a global vent distribution consistent with the model prediction, except for the sections close to the St-Paul-Amsterdam Plateau which appear to be influenced by the eponymous hotspot. East of the AAD, a variety of observations suggests the presence of an area probably as anomalous as the AAD itself. The shallow residual basement depth [e.g., *Marks et al*., 1990; *Whittaker et al*., 2010], off-axis volcanism, and the presence of westward propagators [*Phipps Morgan and Sandwell*, 1994; *Sempéré et al*., 1996; *Briais et al*., 2009a] suggest that the magma production under the South Tasmania SEIR section is not only larger than the cold AAD area, but also abnormally high compared to other sections of intermediate-spreading MORs such as the Juan de Fuca Ridge [*Briais et al*., 2009b].

In addition to the regional magma budget, the diversity of geological contexts along the SEIR, as for instance the stretched lithosphere near the propagator tips or other axial discontinuities such as the George V large-offset Fracture Zone (FZ), may favor fluid circulation within the seafloor, possibly interacting with ultramafic rocks and hence, providing fluids with potentially contrasted chemical compositions. As a result, a major objective of the survey that we carried out between 130 and 140°E was to better understand how and to which extent the variety of geological settings and features observed on the SEIR may influence the occurrence of potential hydrothermal sites, thereby the type of venting.

Here we report the first results of a systematic exploration for hydrothermal plume occurrences along ~700 km of the SEIR between 130°E and 140°E, confirming the presence of hydrothermal activity. During the STORM cruise on board *N/O L'Atalante* (31 December 2014 to 5 February 2015) [*Briais and STORM Cruise Science Party*, 2015], we used a combined approach of seafloor mapping, *in situ* water column chemical measurements and sampling together with rock dredges. The results allowed us not only to find chemical evidence for high-temperature hydrothermal venting all along the SEIR axis in relation with high magma supply, but also to identify plumes likely linked to serpentinization in the George V FZ and possibly along the axis, which would be the first occurrence of ultramafic-derived fluid flow along an intermediate spreading ridge.

2. Study Area

The SEIR was created during the late Cretaceous ~85 Ma ago by the rifting of the Gondwana [*Veevers et al*., 1991]. The spreading between Australia and Antarctica remained ultra-slow and oblique until the mid-Eocene, increasing to intermediate rate ~43 Ma ago in a main NNE-trending direction after the major plate reorganization in the Indian Ocean. Since then, the full opening rate has remained stable, from 59 to 75 mm/yr along the whole ridge [*Royer and Sandwell*, 1989; *DeMets et al*., 2010].

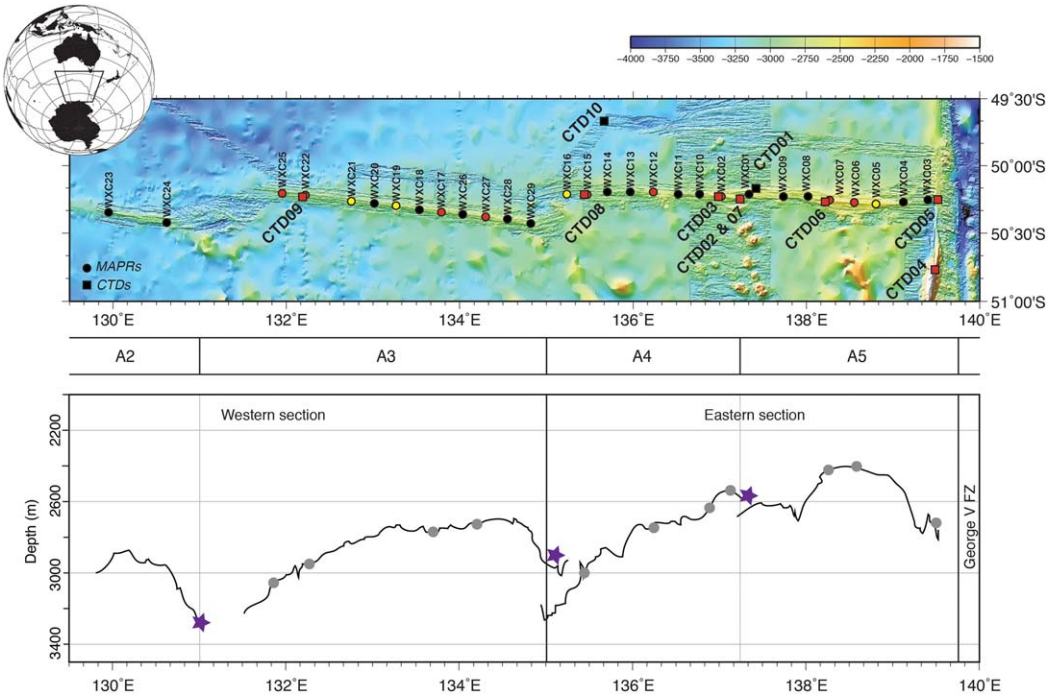

Figure 1. (top) High-resolution bathymetry of the axial area acquired during the STORM cruise showing stations where MAPRs (circles) and CTDs (squares) profiles were carried out. Red color indicates inferred hydrothermal vents, yellow color potential hydrothermal signal. Note that CTD 10 was carried out off-axis for background reference. CTD 04 was performed on a massif in the George V large-offset FZ that appeared to be a serpentinite massif based on rock dredge samples. Bottom: Axial bathymetry profile of the 130–140°E section of the SEIR relative to longitude. Plain circles indicate the locations of the hydrothermal plumes (CTD and MAPR casts); purple stars indicate the location of the OSCs.

The study area, between 130°E and 140°E, is located on the SEIR segments southwest of Tasmania, east of the AAD, along the 50°S parallel (Figure 1). The change of axial morphology between the AAD and the 130°E–140°E section of the SEIR (called "Zone A" in previous works [*Weissel and Hayes*, 1974]) is abrupt just west of the 128°E transform fault [*Sempéré et al*., 1996; *Christie et al*., 1998]. This transform fault also corresponds to a major geochemical isotopic boundary between MORBs derived from the Indian mantle and those derived from the Pacific mantle [*Klein et al*., 1988; *Christie et al*., 1998; *Kempton et al*., 2002]. West of the 128°E transform fault, the AAD is characterized by a deep, broad axial valley with a high relief, while the 130°E–140°E section of the SEIR features a 10 km wide-, 500 m-high domed axis with a low relief (200–400 m variations), as is generally observed for fast-spreading ridges [*Sempéré et al*., 1996]. In our study area, the axis itself is relatively straight, but is offset at 131°E and 135°E by two large-offset overlapping spreading centers (OSCs) propagating westward. A smaller OSC at 137°17′E was revealed during our survey [*Briais and STORM Cruise Science Party*, 2015]. These OSCs define four second-order ridge segments, named A2–A5 from west to east following *Sempéré et al*. [1996] (Figure 1).

East of ∼133°E, the satellite-derived free-air gravity anomaly map [*Sandwell and Smith*, 1997, 2009] reveals a zone on the ridge flank, where many oblique structures are observed, some of them forming V-shapes, associated with active propagating rifts pointing to the west (Figure 1) [*Phipps Morgan and Sandwell*, 1994; *Sempéré et al*., 1996], others, only observed on the southern ridge flank, likely associated to volcanic ridges [*Briais et al*., 2009a]. The George V Transform Fault system at 139°30′E marks the eastern limit of our study area. It offsets the axis by 300 km and is the first in a series of large-offsets, right-stepping transform faults separated by intra-transform ridge segments which were only partly surveyed during the STORM cruise.

During the STORM cruise, we collected multibeam bathymetry, imagery, and magnetics in two high-resolution survey areas: one covering seafloor aged approximately 10 Ma to the south and 5 Ma to the north of the SEIR, and including several off-axis volcanic ridges, the second covering the intersection of the SEIR with the George V Transform Fault, and part of two intra-transform ridge segments. We also mapped the ridge axis as far west as 130°E. We dredged the off-axis volcanoes and the substratum of the transform

fault system, and we collected basalt glass samples with rock-core (wax-core) along the ridge axis. The multibeam-bathymetry maps reveal that the ridge axial segments are shallower to the east and deepen to the west (Figure 1). The easternmost segment A5 shows a relatively shallow axial ridge, suggesting a robust magma supply. Mapping and sampling of the northern part of the George V transform fault system has revealed that a transpressive tectonic massif is being emplaced along the transform, similar to the one described on the slow-spreading Mid-Atlantic Ridge at the St. Paul transform fault [*Maia et al*., 2016]. It forms a NS-trending massif, and appears to result from a compressive component of the motion along the transform fault. As described later, samples from two dredges along the bathymetric high consist of serpentinites.

3. Materials and Methods

As part of the STORM Cruise, which primarily aimed at mapping and rock sampling the 130–140°E section of the SEIR and the off-axis structures, water column profiles were carried out along the four second-order segments and in the George V FZ to identify any hydrothermally related physical and chemical anomalies (Figure 1). Ten of them were performed with a CTD-rosette package and 25 by Miniature Autonomous Plume Recorders (MAPRs) attached to the wire on rock cores (waxcores). MAPRs were also deployed during the CTD-rosette operations.

3.1. Instrumentation and Data Acquisition

High-resolution bathymetry was acquired along the ~1000 km axis using the ship's EM122 multibeam echo sounder (Konksberg), operating at a frequency of 12 kHz allowing seabed mapping to full ocean depth. Waxcore/MAPRs sites were chosen based on the high-resolution bathymetry to sample the ridge axis at regular intervals. We selected the location of CTD-rosette profiles among the MAPR profiles displaying plume-like anomalies except for CTD04, which was located in a different geological setting with strong suspicion of low-temperature venting. CTD10 was carried out off-axis as a background reference.

MAPRs are small, self-contained units including a CTD package, an Eh sensor (measuring oxidation-reduction potential) and a light-backscatter sensor for the nephelometric turbidity. The Eh sensor––also called ORP sensor––is highly sensitive to the presence of reduced chemicals such as Fe^{2+}, H_2 and H_2S [*Walker et al*., 2007] that are characteristic of deep-sea 'black smoker' plumes. ORP anomalies are negative and are rarely found farther than ~1 km from the source [*German et al*., 2008; *Baker et al*., 2010, 2014].

The CTD-rosette package consisted in a SeaBird 911+ fitted with 16 8L-NISKIN bottles and various sensors for conductivity, temperature and pressure as well as two Seapoint Turbidity Meters (STM), which allowed for the detection of high concentration of suspended particulate material. The novel feature of this package was the use – for the first time on a rosette – of an *In Situ* Mass Spectrometer (ISMS) for real-time, *in situ* measurements of dissolved gas concentrations including H_2, CH_4 and CO_2. The instrument, developed at Harvard University (Girguis Lab) and adapted from *Wankel et al*. [2010] for water column measurements, is made of three components: a gas-permeable membrane inside an inlet resisting to pressure up to 600 bars, a turbo-molecular pump allowing a vacuum of 10^{-10} Torr and a Residual Gas Analyser which can scan masses up to 300 MU. In order to lower the detection limits of the ISMS and to adapt the instrument to water column measurements, the membrane inlet was optimized, and the introduction system equipped with a water trap. The configuration and the optimization of the instrument will be detailed in a future technical note.

Data from the ISMS were transmitted via a self-supporting electro-cable to a Seabird SBE11+ Deck Unit and computed using homemade software, while energy for the ISMS was provided by a Li-ion battery pack specifically designed to meet the power requirements of the instrument. The homemade software was designed not only to collect and compute the data from the ISMS but also to transmit orders such as starting the instrument (both turbomolecular pump and the Residual Gas Analyser) and firing the NISKIN bottles. Real-time data from the CTD and Turbidity sensors were transmitted to the same Deck Unit and computed using the SeaSave software with the usual data correction as recommended by Seabird. Outliers, especially for the turbidity, were discarded by comparing the measured values with local averages.

CTD-rosette vertical profiles were conducted throughout the water column, stopping ~5 m above the seafloor, in a single trip. For one station (CTD07), a towed vertical and horizontal profile was performed to track

the strongest turbidity anomaly around the inferred location of a vent site. When a hydrothermal plume was suspected from the nephelometry and temperature sensors, bottles were fired on the way up in order to intercept the bottom, the centre and the top of the hydrothermal plumes with a high resolution (~20 m), as well as to get seawater samples below and above the plumes.

3.2. Sampling and Analytical Methods

Water samples were taken from standard 8L NISKIN bottles, fitted with Teflon stopcocks and sealed with Viton O-rings, both compatible with metal analyses. All water samples were processed identically straight after the CTD-rosette back on board the N.O. *L'Atalante*. Airtight glass ampoules for dissolved gas analyses were flushed with the water from the NISKINS, filled until overflow, poisoned, and sealed to avoid any air contamination. Aliquots were taken into acid washed Nalgene flasks and acidified for total dissolved manganese (Mn) analyses back onshore.

Dissolved methane concentrations were determined onshore using the purge-and-trap technique followed by conventional gas chromatography analysis [*Charlou et al*., 1988; *Charlou and Donval*, 1993]. The detection limit of this technique is 22 pM and the limit of quantification is 75 pM with 5% precision. Due to logistical constraints, it was not possible to perform the gas analysis on board, shortly after the sample recovery. This led to an under-estimation of the real concentrations which can be corrected with the *in situ* data acquired via the ISMS.

Mn concentrations were analyzed with a Thermo Element 2 High Resolution Inductively Coupled Plasma Mass Spectrometer (ICP-MS) at the Pôle de Spectrométrie Océan (PSO, Brest, France). All samples were diluted 30 times in MQ water and spiked with the same amount of Indium in order to correct for instrumental mass discrimination. The precision of analyses was better than 10%, and reached 2% for the most enriched samples. All Mn concentrations were blank and instrumental-drift corrected with a detection limit of 0.5 nM and a quantification limit of <1 nM.

4. Results and Discussion

4.1. Plume Signatures Detected in the George V Fracture Zone

One of the most significant results of our survey was the identification of plume signatures in the water column above the NS-trending bathymetric high located along the western segment of the George V FZ (Figures 1 and 2, left). The dredge 18 carried out at the summit of the massif sampled consolidated to semi- and un-consolidated breccia made of highly altered mafic and ultramafic rock fragments embedded in a matrix of serpentine-chlorite mud. Some pieces of the consolidated breccia have a deep reddish color attributable to an oxidizing environment. Many fragments appear to be rich in magnetite (they attract the compass). Elements of the breccia have angular shape and range in size from a few centimeters to several decimeters. They belong to two main lithological types: serpentinites and metabasalts. Metabasalts derive from olivine phenocrysts-rich lavas with variable but generally low content of plagioclase phenocrysts. Serpentinites derive most likely from mantle peridotites although the 100% degree of serpentinization makes the precise determination of the protolith quite tricky. When not fully erased by serpentinization, the texture of the former peridotite appears to be coarse grained. Some fragments contain former pyroxenes porphyroclasts (now bastites, likely after orthopyroxene, consistent with a harzburgitic protolith). No evidence for mylonitization prior to alteration has been found in the rock fragments. By the same way, the collected samples do not show evidence for shearing after the formation of the breccia whose origin is probably to be looked for in rather shallow processes (slope debris?). The presence of serpentinized peridotites infers the transpressive nature of the bathymetric high enabling exhumation of mantle rocks as well as the alteration consequence of seawater circulation through ultramafic rocks.

The absence of backscatter/turbidity anomalies at this station (Figure 2, right) provides strong evidence that the observed signal in the water column is not representative of a high-temperature hydrothermal vent, which would be unlikely in this setting. However, the presence of a significant CH_4 anomaly (up to 2 nmol/L) associated to a subtle but still significant Eh decrease (2 mV) tends to prove that the signal is most likely originating from a low-temperature hydrothermal circulation. Indeed, Eh is sensitive to the presence of reducing chemicals such as H_2, which might be present in the water column at significant concentrations as was shown for the Lost City hydrothermal vent [*Larson et al*., 2015]. Furthermore, the alteration, known

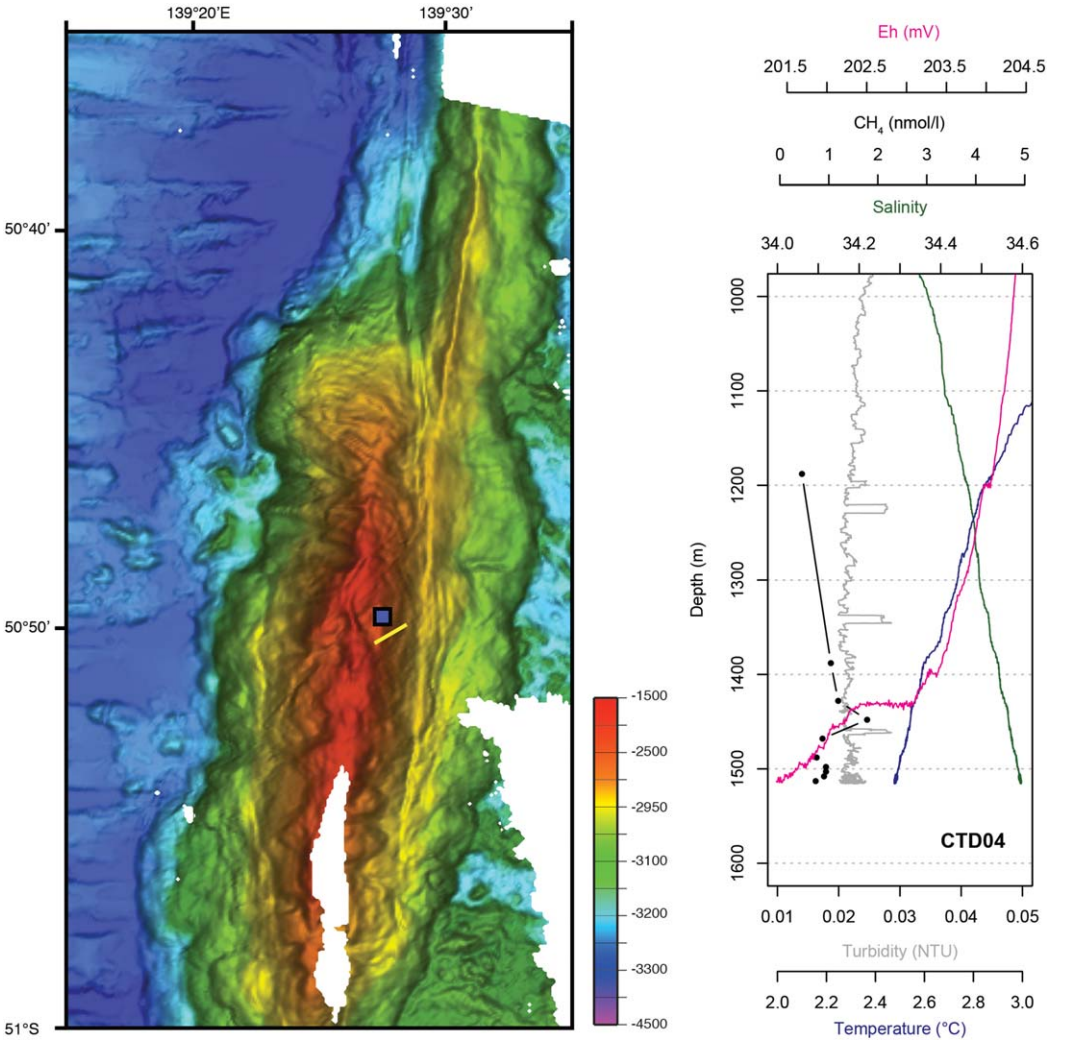

Figure 2. (left) High-resolution bathymetry of the serpentinite massif in the George V FZ, showing the location of the CTD hydrocast (blue square) and the dredge path (yellow line). (right) Vertical profiles of hydrothermal tracers for CTD04 showing a slight decrease of redox potential correlated to a small but significant CH_4 anomaly at ~1440 mbsl.

as the serpentinization, leads to the production of H_2, which subsequently reacts with the CO_2 to produce CH_4 [*Charlou et al.*, 2002; *Proskurowski et al.*, 2006]. This reaction can explain the presence of the CH_4 anomaly in the water column without the backscatter/turbidity anomaly usually observed at high-temperature hydrothermal sources [*Charlou et al.*, 1991]. Unfortunately, no H_2 signals were recorded with the *in situ* mass spectrometer, probably related to the difficulty to detect such highly volatile gas in the aqueous phase together with the high detection limits of the instrument ($>1\mu M$). Nonetheless, the combined Eh and CH_4 anomalies are the most unambiguous evidence of ultramafic-related fluid flow in the George V FZ massif.

A famous example of such hydrothermal fluid circulation is from the Lost City Hydrothermal Field on the Atlantis Massif that is located at the intersection between the MAR and the 75 km-offset Atlantis transform fault (30°N) [*Kelley et al.*, 2001]. The surface of the Atlantis massif is interpreted to be a major low-angle detachment fault, which exhumes mantle peridotite to the surface. However, in our study area the location and morphology of the serpentinite massif along the transform fault suggest that it results from a compressive component along the strike-slip fault, implying processes likely to favor the uplift of deep crust and mantle rocks, in the same way as described in the St. Paul transform fault [*Maia et al.*, 2016]. Another example of ultramafic outcrop along a transform fault, at the fast-spreading East Pacific Rise, is described along the Garrett Transform Fault, but the cause for the uplift of deep rocks is not well explained [*Hekinian et al.*, 1992]. Further

investigations need to be devoted to tectonic processes and hydrothermal circulation in the area as the proximity of venting is now clearly evidenced.

4.2. Plume Signatures Along the Ridge Axis

4.2.1. MAPR Survey

Along the four segments of the surveyed SEIR section, 29 MAPR profiles were acquired during waxcore operations, revealing anomalies in the water column for several of them (Figure 1) with clear Eh and turbidity signals close to the bottom seafloor on descending profiles, i.e., with no possible influence of resuspended sediments when the waxcore hits the seafloor. From the data, strong physical and chemical signals suggesting a close by plume are not evenly distributed along the axis as distances between two anomalies may vary from 35 to 112 km along the axis, with an average of 70 km. The number of sites (including unconfirmed anomalies) is 1.8 per 100 km, a value slightly lower than the predicted value of 2.25 calculated from the empirical relationship presented in *Beaulieu et al*. [2015]. This is expected on an intermediate-spreading ridge, and confirms that the primary control of the hydrothermal activity of these segments is magmatic. The small discrepancy might be due to the relatively loose spacing of the profiles, of 10 n.m.

All these primary observations, together with the bathymetry, define two distinct sections: (1) the eastern one delimited by the George V FZ and the 135°E offset and 2) the western one stretching the area between the 135°E offset and the AAD at 128°E. In the eastern section, where most of the anomalies were found, the ridge axis is shallow and inflated (Figure 1), indicating a higher melt supply, and hence higher mantle temperatures [*Briais et al*., 2009a]. In comparison, the westernmost ridge axis is deeper and less inflated (Figure 1). The ridge morphology is a good indicator of the mantle temperature that regulates the magma supply to the crust [*Sempéré et al*., 1996; *Cochran and Sempéré*, 1997]. Our observations, very similar to *Baker et al*.'s [2014] close to the Amsterdam-St Paul plateau as well as to *Hahm et al*.'s [2015] on the AAR, confirm that the change of mantle temperature along the segments not only regulates the magma supply, but also impacts the occurrences of potential hydrothermal sites, in the same way as along the superfast spreading EPR [*Baker et al*., 2002].

4.2.2. CTD-Hydrocast Survey

To confirm the distinction between the two provinces, we picked locations for CTD hydrocasts based on bathymetry and MAPR data. Figure 3 presents the CTD-hydrocast profiles all along the investigated segments of the SEIR together with the off-axis profile of CTD10 considered to be the seawater reference for the area. CTD10 shows that deep water-masses are characterized by low salinity (34.6) and temperature (∼1.5°C), which define the Antarctic Bottom Waters (ABW) [*Mantyla and Reid*, 1983]. In this area, the bottom waters circulation is constrained both topographically by the EW-trending SEIR system and dynamically by the Circumpolar Current [*Mantyla and Reid*, 1983].

4.2.2.1. Eastern Section: 135°E - OSC to 140°E - George V Fracture Zone

First, we chose the CTD hydrocast locations based on the high-resolution bathymetry highlighting structures such as fractures, topography highs, and volcanoes in the axial area that were likely to host hydrothermal vent sites, as previously observed on mid-ocean ridges [*Baker et al*., 2001]. The first hydrocast (STRM-CTD01), carried out on the northern flank of a topographic high on the axis, did not reveal any physico-chemical anomaly. However, within the small basin separating the axial tips of the 137°17'E OSC (which we named "La piscine"), strong signals on the nephelometer, temperature and conductivity sensors were detected during the second CTD hydrocast (STRM-CTD02, Figure 3). The turbidity anomaly of 0.02 NTU as well as the temperature anomaly of ∼0.1°C indicate that the rosette was lowered in the vicinity of an active vent. The MAPR attached to the CTD frame confirmed the presence of the plume with strong Eh (5 mV) and salinity (∼0.003 units) anomalies. Figure 4 shows the vertical CH_4 and Mn profiles (measured *in situ* and in water samples, respectively) with concentrations up to 25 nmol/L and 12 nmol/L respectively. This station was reoccupied later on during the STRM-CTD07 hydrocast with the aim to intercept the plume and locate the source. Note that the profile shown in Figure 3 was obtained after the strongest turbidity signal was found. The highest turbidity anomaly had a peak centred at ∼120m above the seafloor, slightly lower than STRM-CTD02 with a thickness of 200 m (Figure 3). The maximum (ΔNTU=0.025) is clearly correlated to a temperature anomaly of >0.1°C and a slight salinity anomaly at the same depth, which indicates that the CTD-rosette was close enough to an active vent. Concentrations of dissolved CH_4 recorded by the ISMS are up to 25 nM, which are consistent with the analyses performed on the water samples, while Mn concentrations are up to 30 nM. All these chemical signatures, significantly different from the background STRM-

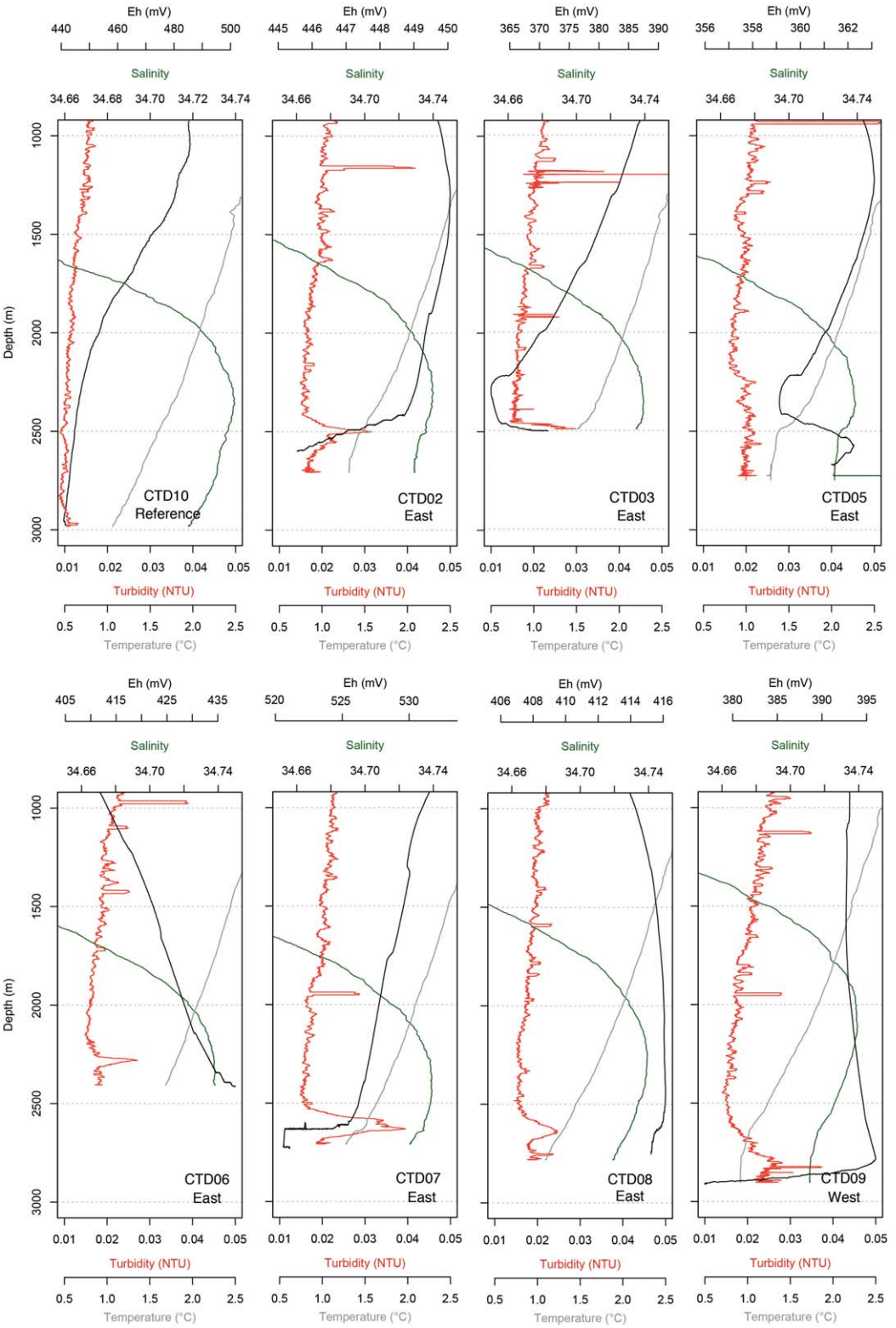

Figure 3. Vertical profiles of hydrothermal tracers (temperature, salinity, turbidity and redox potential) along the axis. CTD10 is the reference profile for the area. Note that Eh scale is different in each plot for clarity.

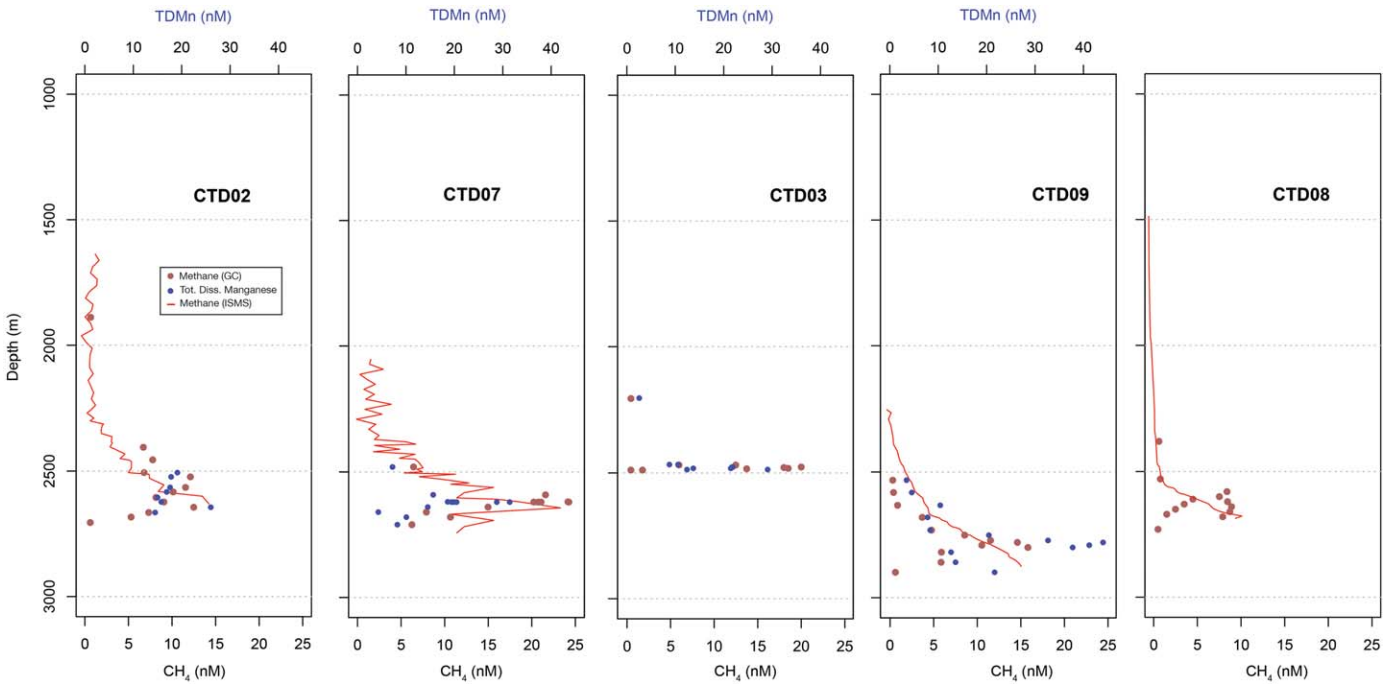

Figure 4. Vertical profiles of Mn (blue dots) and CH_4 (red dots for samples and red line for ISMS measurements) indicating the presence of methane (CH_4) and manganese (Mn) anomalies for CTD02, 03 and 09. Note that the limits of quantification are $<$1 nM and 75 pM for Mn and CH_4 respectively. Mn data for CTD08 are not available.

CTD10 hydrocast (Figure 3), confirm the occurrence of a hydrothermal source close to the actual CTD-rosette location. A dredge in the area allowed the recovery of hydrothermally altered basalts but no hydrothermal deposits such as chimney or fauna was found in the dredge bag. The site is located on the inner flank of a small structure that appears to be a volcano within a small-offset OSC basin. Although uncertainty remains on the exact and precise location of the vent – as it was impossible to evaluate current direction at the time of the cast – the current data should allow to track the sources in one single dive.

The third CTD hydrocast (STRM-CTD03) was carried out at the same location as WXC02, where the presence of a plume was inferred from the MAPR profile. The plume is very close to the seafloor ($<$50 m above) but Mn and CH_4 concentrations, up to 30 nM and 20 nM respectively, and correlated to the nephelometry and Eh anomalies, clearly indicate the hydrothermal origin of the plume (Figure 4). Due to the distance between STRM-CTD02/07 and STRM-CTD03 (15 km) and the presence of the Eh anomaly, the signal recorded at CTD03 cannot originate from the same vent as the one responsible for the STRM-CTD02/07 signal, but from a vent located within a range of $\sim$1 km of the STRM-CTD03 hydrocast position.

STRM-CTD05 was carried out on a flank of a topographic high at the very end of the axis, close to the George V transform fault zone, 5 km east of the WXC03 location. A weak turbidity signal $<$0.01 NTU was found, which could not be confirmed by additional anomalies, (e.g., temperature) despite the 0.011 NTU anomaly spotted by the MAPRs on the nearby WXC03. Yet, the Eh profile is not typical of a hydrothermal anomaly.

STRM-CTD06 revealed the presence of turbidity (0.01 NTU). The plume detected at this location is centred at 2300 m depth, about 200 m above the seafloor, with a thickness of $\sim$100 m. The absence of Eh anomalies indicates that the source is located more than 1km away from the hydrocast station (Figure 3). The even weaker signal at WXC07 suggests that the source was in fact located further east, likely close to WXC06, which was $\sim$23 km east of CTD06. At WXC06, the presence of an Eh anomaly clearly argues for a hydrothermal source in close vicinity. The inferred source for STRM-CTD06 plume signals is probably located on the axis whose robust dome-like shape suggests the presence of a magma lens very close to the surface.

Despite the absence of a clear signal on the WXC15 MAPR profile carried out at the same location, STRM-CTD08 revealed a plume at 2650 m (centre of the plume) with a thickness of $\sim$150 m, and $\sim$200 m above the seafloor. The Eh profile indicates an anomaly at 2650 m depth, which confirms the presence of a

hydrothermal vent less than 1km from the station. Furthermore, there is a strong correlation of the Eh values with the dissolved methane concentrations that reached ~9 nM in the centre of the plume (Figure 4).

4.2.2.2. Western section: 130°E to 135°E - OSC

STRM-CTD09 hydrocast was carried out at the same location as WXC22, where MAPR profile had revealed a 0.02 NTU turbidity anomaly and a strong Eh signal (>15 mV anomaly). Concentrations for CH_4 and Mn reach up to 16 nM and 40 nM, respectively.

Due to adverse weather conditions, it was not possible to investigate any further along this segment with hydrocast lowerings. However, MAPR profiles acquired during waxcore operations suggest that hydrothermal venting is most likely more frequent than the observations acquired during the course of this survey. It would be valuable to carry out a CTD hydrocast around the WXC17 location, which showed Eh and NTU as well as physico-chemical anomalies similar to those obtained on WXC22 depth profile.

4.3. Chemical Compositions of the Plumes

Based on our new data set for the most prominent hydrocasts, we calculated the CH_4:Mn ratios for each plume and compared them with other worldwide vent systems (Figure 5). Note that we took only the samples from the middle of the plumes, excluding top and bottom of the plumes as the reactivity of Mn and CH_4 is different. Indeed, CH_4 tends to be oxidized more rapidly than Mn [*Ishibashi et al.*, 1997; *Kawagucci et al.*, 2008]. Interestingly the ratios appear to vary from a plume to another from 0.37 (CTD09) to 0.65 (CTD07), suggesting different underlying hydrothermal type of venting. In particular, the comparison with other well-known vents shows that at least two––perhaps three––types of hydrothermal circulation occur on the SEIR. The first type represented by STRM-CTD09 is characterized by a low CH_4:Mn ratio of 0.37 similar to that obtained for the EPR or the TAG vent site on the MAR [*Charlou et al.*, 1991; *Ishibashi et al.*, 1997]. For this station, located on the top of the inflated axis, we propose that the underlying source is a typical high-temperature, black-smoker vent, characterized by high-particle content confirmed by the 0.02 NTU anomaly, high Mn and low CH_4 concentrations. This would suggest that this site is hosted on basalts as evidenced by fresh basalt glasses recovered from WXC22. The second type, represented here by the STRM-CTD02/07 is characterized by a rather high CH_4:Mn ratio at 0.65, very similar to the one calculated for the Rainbow plume on the MAR [*German et al.*, 2009]. Rainbow is an ultramafic-hosted, high-temperature vent featuring very high concentrations of CH_4 and H_2 due to the circulation of water through ultramafic rocks [*Charlou et al.*, 2002]. In our case, the nearby but single STRM-DR16 dredge did not recover ultramafic rocks from the seafloor, only basalts, but the fractures and faults associated with the OSC might provide a pathway for seawater to reach the underlying mantle rocks and then react to produce H_2. This could be supported by the presence of ultramafic fluid flow found in the George V FZ and therefore an influence of the serpentinization process on the chemical composition of the fluids at the segment scale. An alternate hypothesis would be that active degassing from underneath magma chambers could generate high volatile:metal ratios in the fluids. One might think that high volatile degassing could generate high CH_4 to Mn ratios, although in typical magmatic systems, CO_2 dominates the vapor phase [*Resing et al.*, 2004]. The ongoing study of the composition of the underlying basalts will allow a better description of the fluid

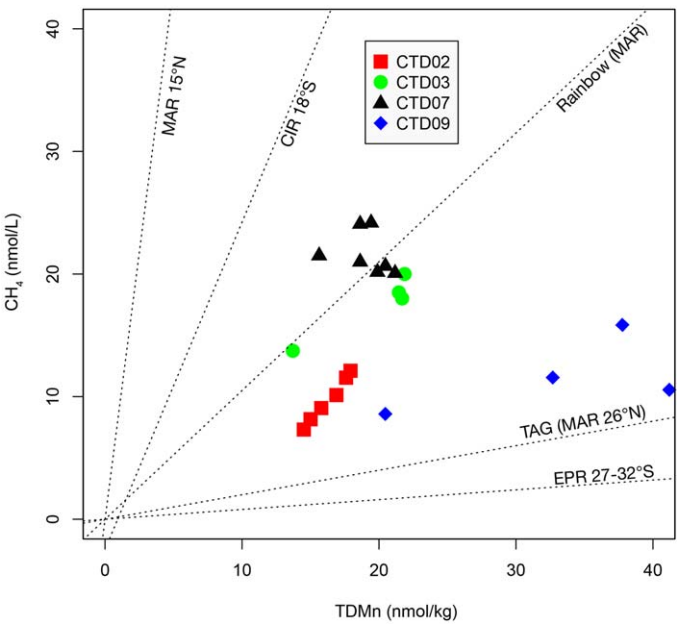

Figure 5. Dissolved CH_4 versus TDMn concentrations for CTD02, 03, 07, and 09. Only samples from the middle of the plume were taken for this plot. The dashed lines show the trends for MAR 15°N [*Charlou et al.*, 2002], CIR18°S [*Kawagucci et al.*, 2008], TAG (MAR 26°N) [*Charlou et al.*, 1991] and EPR 27–32°S [*Gharib et al.*, 2005].

pathway and therefore, of the chemical reactions generating such variability. The very high turbidity anomaly as well as the high concentration of Mn definitely exclude a low temperature hydrothermal activity, such as Lost City [*Kelley et al*., 2001] but point to a high-temperature one instead. The CH_4 enrichment of the water samples also supports the hypothesis that fluids are dominated by the vapor-phase (with high concentrations of dissolved gases), which could be an indication for a recent volcanic activity [*Von Damm et al*., 2003].

5. Conclusions

The exploration for hydrothermal venting along the SEIR and within the George V FZ revealed for the first time evidence for ultramafic-related fluid flow on an intermediate-spreading ridge. The CH_4 and Eh anomalies detected in the water column above a highly altered peridotite massif in the George V FZ are unambiguously due to the serpentinization process, leading to the production of H_2 and subsequently of CH_4. This discovery expands the possibility for ultramafic circulation along the global ridge-crest, and not only along slow to ultraslow-spreading ridges.

The exploration along the SEIR axis revealed that the hydrothermal activity is controlled by magmatic processes at the segment scale. Our observations indicate that the change of mantle temperature along the investigated segments not only regulates the magma supply but also the hydrothermal activity and the type of venting. Therefore, two distinct sections can be defined: 1) the George V FZ to 135°E offset where the ridge is inflated and shallow and 2) the 135°E offset to the AAD where the ridge is deeper and less inflated.

Overall, the chemical characteristics of hydrothermal plumes along the SEIR axis suggest that at the local scale, tectonics might play an important role to explain the differences of CH4:Mn ratios from a station to another. Clearly, the geological settings influence the type of circulation, from crustal to ultramafic.

Our data along the investigated segments suggest a significant high-temperature hydrothermal activity, characterized by strong turbidity anomalies, and hence indicate a strong particle input in the water column. Beyond these results, the STORM cruise highlighted the intense hydrothermal activity on the SEIR which could be an important source of elements to the global biogeochemical cycles [e.g., *German et al*., 2016b]. As attested by the high Mn concentrations, this input could be an important source of micronutrients, especially in the Southern Ocean where Fe inputs are limited. Finally, studying the occurrence of hydrothermal venting along the SEIR is a prerequisite for a better understanding of the biogeography in the Southern Ocean [e.g., *Van Dover*, 2002; *Moalic et al*., 2012], which is an important component for biological connectivity between Pacific, Indian and Atlantic Oceans.

Acknowledgments
This work was funded by CNRS/INSU STORM Cruise Program (PI A. Briais). Participation of C. Boulart, water sampling, chemical analyses, and deployment of the *In Situ* Mass Spectrometer were supported by the French National Research Agency (ANR) HOTPLUME grant (ANR-13-PDOC-0020). The authors thank Peter Guirgis and Charles Vidoudez (Harvard University) for their help in the optimization of the *In Situ* Mass Spectrometer for water column measurements. Real-time control of the ISMS and its adaptation on the CTD-rosette were possible thanks to Michel Lunven, Anne Guillemot, Dominique Birot, and Jonathan Perchoc (Ifremer). The authors also thank Sharon Walker and Ed Baker (NOAA) for MAPR expertise as well as Cécile Cathalot and Cécile Konn (Ifremer) for their useful comments on the manuscript. This work would not have been possible without the support and help of the Captain and crew of RV *L'Atalante* in the challenging conditions of the Furious Fifties. Finally, the authors thank the anonymous reviewer and C. R. German for their constructive reviews, which greatly improved the initial manuscript. Locations for MAPR profiles can be found in supporting information Table S1. CTD locations, Mn and CH_4 concentrations are given in supporting information Table S2. Complementary MAPR and CTD profiles as well as chemical data are available by request to CB and additional data for bathymetry by request to AB.

References

Baker, E. T., and C. R. German (2004), On the global distribution of hydrothermal vent fields, in *Mid-Ocean Ridges: Hydrothermal Interactions Between the Lithosphere and Oceans*, edited by C. R. German, J. Lin, and L. M. Parson, pp. 245–266, Geophysical Monograph Series, Washington, D. C.

Baker, E. T., C. R. German, and H. Elderfield (1995), Hydrothermal plumes over spreading-center axes: Global distributions and geological inferences, in *Seafloor Hydrothermal Systems: Physical, Chemical, Biological, and Geological Interactions*, vol. 91, edited by S. E. Humphris et al., pp. 47–71, AGU, Washington, D. C.

Baker, E. T., M.-H. Cormier, C. H. Langmuir, and K. Zavala (2001), Hydrothermal plumes along segments of contrasting magmatic influence, 15°20′-18°30′N, East Pacific Rise: Influence of axial faulting, *Geochem. Geophys. Geosyst.*, *2*(9), 1051, doi:10.1029/2000GC000165.

Baker, E. T., et al. (2002), Hydrothermal venting along Earth's fastest spreading center: East Pacific Rise, 27.5°-32.3: Hydrothermal venting on the East Pacific rise, *J. Geophys. Res.*, *107*(B7), 2130, doi:10.1029/2001JB000651.

Baker, E. T., F. Martinez, J. A. Resing, S. L. Walker, N. J. Buck, and M. H. Edwards (2010), Hydrothermal cooling along the Eastern Lau Spreading Center: No evidence for discharge beyond the neovolcanic zone: Hydrothermal Cooling On and Off Axis, *Geochem. Geophys. Geosyst.*, *11*, Q08004, doi:10.1029/2010GC003106.

Baker, E. T., C. Hémond, A. Briais, M. Maia, D. S. Scheirer, S. L. Walker, T. Wang, and Y. J. Chen (2014), Correlated patterns in hydrothermal plume distribution and apparent magmatic budget along 2500 km of the Southeast Indian Ridge, *Geochem. Geophys. Geosyst.*, *15*, 3198–3211, doi:10.1002/2014GC005344.

Beaulieu, S. E., E. T. Baker, and C. R. German (2015), Where are the undiscovered hydrothermal vents on oceanic spreading ridges?, *Deep Sea Res., Part II*, *121*, 202–212, doi:10.1016/j.dsr2.2015.05.001.

Briais, A., and STORM Cruise Science Party (2015), *Structure and Dynamics of the Southeast Indian Ridge and Off-axis Volcanism, 129°E to 140°E: Preliminary Results of the STORM Cruise*, p. V14A–02, AGU, San Francisco, Calif.

Briais, A., O. Gomez, and R. Lataste (2009a), *Evidence for off-axis Seamounts on the Flanks of the Southeast Indian Ridge, 128°E-150°E. Implications for Mantle Dynamics east of the Australia-Antarctic Discordance*, vol. 11, 11869 pp., EGU General Assembly, Vienna.

Briais, A., H. Ondréas, F. Klingelhoefer, L. Dosso, C. Hamelin, and H. Guillou (2009b), Origin of volcanism on the flanks of the Pacific-Antarctic ridge between 41°30′S and 52°S: Pacific-Antarctic Ridge Off-Axis Volcanism, *Geochem. Geophys. Geosyst.*, *10*, Q09001, doi:10.1029/2008GC002350.

Charlou, J.-L., and J.-P. Donval (1993), Hydrothermal methane venting between 12°N and 26°N along the Mid-Atlantic Ridge, *J. Geophys. Res.*, *98*, 9625–9642.

Charlou, J. L., L. Dimitriev, H. Bougault, and D. Needham (1988), Hydrothermal CH4 between 12° and 15° N over the Mid-Atlantic Ridge, *Deep Sea Res., Part A*, *35*, 121–131.

Charlou, J. L., H. Bougault, P. Appriou, T. Nelsen, and P. Rona (1991), Different TDM/CH4 hydrothermal plume signatures: TAG site at 26°N and serpentinized ultrabasic diapir at 15°05′N on the Mid-Atlantic Ridge, *Geochim. Cosmochim. Acta*, *55*(11), 3209–3222.

Charlou, J. L., J. P. Donval, Y. Fouquet, P. Jean-Baptiste, and N. Holm (2002), Geochemistry of high H2 and CH4 vent fluids issuing from ultramafic rocks at the Rainbow hydrothermal field (36°14′N, MAR), *Chem. Geol.*, *191*(4), 345–359.

Charlou, J. L., J. P. Donval, H. Ondreas, Y. Fouquet, P. Jean-Baptiste, and E. Fourre (2010), High production and fluxes of H2 and CH4 and evidence of abiotic hydrocarbon synthesis by serpentinization in ultramafic-hosted hydrothermal systems on the Mid-Atlantic Ridge., in *Diversity of Hydrothermal Systems on Slow-spreading Ocean Ridges*, edited by P. Rona et al., vol. 188, pp. 265–296, Geophysical Monograph Series, Washington, D. C.

Christie, D. M., B. P. West, D. G. Pyle, and B. B. Hanan (1998), Chaotic topography, mantle flow and mantle migration in the Australian–Antarctic discordance, *Nature*, *394*, 637–644, doi:10.1038/29226.

Cochran, J. R., and J.-C. Sempéré (1997), The Southeast Indian Ridge between 88°E and 118°E: Gravity anomalies and crustal accretion at intermediate spreading rates, *J. Geophys. Res.*, *102*, 15,463–15,487, doi:10.1029/97JB00511.

DeMets, C., R. G. Gordon, and D. F. Argus (2010), Geologically current plate motions, *Geophys. J. Int.*, *181*(1), 1–80, doi:10.1111/j.1365-246X.2009.04491.x.

Edmond, J. M., C. Measures, R. E. McDuff, L. H. Chan, R. Collier, B. Grant, L. I. Gordon, and J. B. Corliss (1979), Ridge crest hydrothermal activity and the balances of the major and minor elements in the ocean: The Galapagos data, *Earth Planet. Sci. Lett.*, *46*(1), 1–18.

Elderfield, H., and A. Schultz (1996), Mid-ocean ridge hydrothermal fluxes and the chemical composition of the ocean, *Annu. Rev. Earth Planet. Sci.*, *24*(1), 191–224.

German, C. R., and W. E. Seyfried (2014), Hydrothermal Processes, in *Treatise on Geochemistry*, pp. 191–233, Elsevier.

German, C. R., D. R. Yoerger, M. Jakuba, T. M. Shank, C. H. Langmuir, and K. Nakamura (2008), Hydrothermal exploration with the Autonomous Benthic Explorer, *Deep Sea Res., Part I*, *55*(2), 203–219.

German, C. R., A. M. Thurnherr, J. Knoery, J.-L. Charlou, and H. N. Edmonds (2009), Export fluxes from submarine venting to the ocean: A synthesis of results from the Rainbow hydrothermal field, 36 degrees N MAR, *Geochim. Cosmochim. Acta*, *73*, A428–A428.

German, C. R., S. Petersen, and M. D. Hannington (2016a), Hydrothermal exploration of mid-ocean ridges: Where might the largest sulfide deposits be forming?, *Chem. Geol.*, *420*, 114–126, doi:10.1016/j.chemgeo.2015.11.006.

German, C. R., et al. (2016b), Hydrothermal impacts on trace element and isotope ocean biogeochemistry, *Philos. Trans. R. Soc. A*, *374*(2081), 20160035, doi:10.1098/rsta.2016.0035.

Gharib, J. J., F. J. Sansone, J. A. Resing, E. T. Baker, J. E. Lupton, and G. J. Massoth (2005), Methane dynamics in hydrothermal plumes over a superfast spreading center: East Pacific Rise, 27.5°-32.3°S, *J. Geophys. Res.*, *110*, B10101, doi:10.1029/2004JB003531.

Hahm, D., E. T. Baker, T. Siek Rhee, Y.-J. Won, J. A. Resing, J. E. Lupton, W.-K. Lee, M. Kim, and S.-H. Park (2015), First hydrothermal discoveries on the Australian-Antarctic Ridge: Discharge sites, plume chemistry, and vent organisms: First Hydrothermal Discoveries on AAR, *Geochem. Geophys. Geosyst.*, *16*, 3061–3075, doi:10.1002/2015GC005926.

Hekinian, R., D. Bideau, M. Cannat, J. Francheteau, and R. Hébert (1992), Volcanic activity and crust-mantle exposure in the ultrafast Garrett transform fault near 13°28′S in the Pacific, *Earth Planet. Sci. Lett.*, *108*(4), 259–275, doi:10.1016/0012-821X(92)90027-S.

Hekinian, R., T. Juteau, E. Gracia, B. Sichler, S. Sichel, G. Udintsev, R. Apprioual, and M. Ligi (2000), Submersible observations of Equatorial Atlantic mantle: The St. Paul Fracture Zone region, *Mar. Geophys. Res.*, *21*(6), 529–560.

Ishibashi, J., H. Wakita, K. Okamura, E. Nakayama, R. A. Feely, G. T. Lebon, E. T. Baker, and K. Marumo (1997), Hydrothermal methane and manganese variation in the plume over the superfast-spreading southern East Pacific Rise, *Geochim. Cosmochim. Acta*, *61*(3), 485–500.

Johnson, K. T. M., D. W. Graham, K. H. Rubin, K. Nicolaysen, D. S. Scheirer, D. W. Forsyth, E. T. Baker, and L. M. Douglas-Priebe (2000), Boomerang Seamount: The active expression of the Amsterdam-St. Paul hotspot, Southeast Indian Ridge, *Earth Planet. Sci. Lett.*, *183*(1–2), 245–259.

Kawagucci, S., K. Okamura, K. Kiyota, U. Tsunogai, Y. Sano, K. Tamaki, and T. Gamo (2008), Methane, manganese, and helium-3 in newly discovered hydrothermal plumes over the Central Indian Ridge, 18–20 S, *Geochem Geophys Geosyst*, *9*, Q10002, doi:10.1029/2008GC002082.

Kelley, D. S., et al. (2001), An off-axis hydrothermal vent field near the Mid-Atlantic Ridge at 30°N, *Nature*, *412*, 145–149.

Kempton, P. D., J. A. Pearce, T. L. Barry, J. G. Fitton, C. Langmuir, and D. M. Christie (2002), Sr-Nd-Pb-Hf Isotope results from ODP Leg 187: Evidence for mantle dynamics of the Australian-Antarctic discordance and origin of the Indian MORB Source: HF isotopes and mantle dynamics of the AAD, *Geochem. Geophys. Geosyst.*, *3*(12), 1074, doi:10.1029/2002GC000320.

Klein, E. M., C. H. Langmuir, A. Zindler, H. Staudigel, and B. Hamelin (1988), Isotope evidence of a mantle convection boundary at the Australian-Antarctic Discordance, *Nature*, *333*(6174), 623–629, doi:10.1038/333623a0.

Larson, B. I., S. Q. Lang, M. D. Lilley, E. J. Olson, J. E. Lupton, K. Nakamura, and N. J. Buck (2015), Stealth export of hydrogen and methane from a low temperature serpentinization system, *Deep Sea Res., Part II*, *121*, 233–245, doi:10.1016/j.dsr2.2015.05.007.

Maia, M., et al. (2016), Extreme mantle uplift and exhumation along a transpressive transform fault, *Nat. Geosci.*, *9*(8), 619–623, doi:10.1038/ngeo2759.

Mantyla, A. W., and J. L. Reid (1983), Abyssal characteristics of the World Ocean waters, *Deep Sea Res., Part A*, *30*(8), 805–833, doi:10.1016/0198-0149(83)90002-X.

Marks, K. M., P. R. Vogt, and S. A. Hall (1990), Residual depth anomalies and the origin of the Australian-Antarctic discordance zone, *J. Geophys. Res.*, *95*, 17,325–17,337, doi:10.1029/JB095iB11p17325.

Moalic, Y., D. Desbruyeres, C. M. Duarte, A. F. Rozenfeld, C. Bachraty, and S. Arnaud-Haond (2012), Biogeography revisited with network theory: Retracing the history of hydrothermal vent communities, *Syst. Biol.*, *61*(1), 127–137, doi:10.1093/sysbio/syr088.

Pedersen, R. B., H. T. Rapp, I. H. Thorseth, M. D. Lilley, F. J. A. S. Barriga, T. Baumberger, K. Flesland, R. Fonseca, G. L. Früh-Green, and S. L. Jorgensen (2010), Discovery of a black smoker vent field and vent fauna at the Arctic Mid-Ocean Ridge, *Nat. Commun.*, *1*(8), 126, doi:10.1038/ncomms1124.

Phipps Morgan, J., and D. T. Sandwell (1994), Systematics of ridge propagation south of 30°S, *Earth Planet. Sci. Lett.*, *121*(1–2), 245–258, doi:10.1016/0012-821X(94)90043-4.

Proskurowski, G., M. D. Lilley, D. S. Kelley, and E. J. Olson (2006), Low temperature volatile production at the Lost City Hydrothermal Field, evidence from a hydrogen stable isotope geothermometer, *Science*, *229*(4), 331.

Resing, J. A., J. E. Lupton, R. A. Feely, and M. D. Lilley (2004), CO2 and 3He in hydrothermal plumes: Implications for mid-ocean ridge CO_2 flux, *Earth Planet. Sci. Lett.*, *226*(3–4), 449–464.

Royer, J.-Y., and D. T. Sandwell (1989), Evolution of the eastern Indian Ocean since the Late Cretaceous: Constraints from Geosat altimetry, *J. Geophys. Res.*, *94*, 13,755–13,782, doi:10.1029/JB094iB10p13755.

Sandwell, D. T., and W. H. F. Smith (1997), Marine gravity anomaly from Geosat and ERS 1 satellite altimetry, *J. Geophys. Res.*, *102*, 10,039–10,054, doi:10.1029/96JB03223.

Sandwell, D. T., and W. H. F. Smith (2009), Global marine gravity from retracked Geosat and ERS-1 altimetry: Ridge segmentation versus spreading rate, *J. Geophys. Res.*, *114*, B01411, doi:10.1029/2008JB006008.

Scheirer, D. S., E. T. Baker, and K. T. Johnson (1998), Detection of hydrothermal plumes along the Southeast Indian Ridge near the Amsterdam-St. Paul Plateau, *Geophys. Res. Lett.*, *25*, 97–100.

Sempéré, J.-C., B. P. West, and L. Geli (1996), The Southeast Indian Ridge between 127° and 132°40′E: Contrasts in segmentation characteristics and implications for crustal accretion, in *Tectonic, Magmatic, Hydrothermal and Biological Segmentation of Mid-Ocean Ridges*, vol. 118, edited by C. J. MacLeod, P. A. Tyler, and C. L. Walker, pp. 1–15, Geological Society Special Publication, London, U. K.

Son, J., S.-J. Pak, J. Kim, E. T. Baker, O.-R. You, S.-K. Son, and J.-W. Moon (2014), Tectonic and magmatic control of hydrothermal activity along the slow-spreading Central Indian Ridge, 8°S-17°S, *Geochem. Geophys. Geosyst.*, *15*, 2011–2020, doi:10.1002/2013GC005206.

Tao, C., et al. (2011), First active hydrothermal vents on an ultraslow-spreading center: Southwest Indian Ridge, *Geology*, *40*(1), 47–50, doi:10.1130/G32389.1.

Van Dover, C. L. (2002), Evolution and biogeography of deep-sea vent and seep invertebrates, *Science*, *295*(5558), 1253–1257, doi:10.1126/science.1067361.

Veevers, J. J., C. M. Powell, and S. R. Roots (1991), Review of seafloor spreading around Australia: I. synthesis of the patterns of spreading, *Aust. J. Earth Sci.*, *38*(4), 373–389, doi:10.1080/08120099108727979.

Von Damm, K. L., M. D. Lilley, W. C. Shanks III, M. Brockington, A. M. Bray, K. M. O'Grady, E. Olson, A. Graham, and G. Proskurowski (2003), Extraordinary phase separation and segregation in vent fluids from the southern East Pacific Rise, *Earth Planet. Sci. Lett.*, *206*(3–4), 365–378, doi:10.1016/S0012-821X(02)01081-6.

Walker, S. L., E. T. Baker, J. A. Resing, and K. Nakamura (2007), A new tool for detecting hydrothermal plumes: An ORP sensor for the PMEL MAPR, *Eos Trans. AGU*, *88*(52), Fall Meet. Suppl., Abstract V21D-0753.

Wankel, S. D., S. B. Joye, V. A. Samarkin, S. R. Shah, G. Friederich, J. Melas-Kyriazi, and P. R. Girguis (2010), New constraints on methane fluxes and rates of anaerobic methane oxidation in a Gulf of Mexico brine pool via in situ mass spectrometry, *Deep Sea Res., Part II*, *57*(21–23), 2022–2029, doi:10.1016/j.dsr2.2010.05.009.

Weissel, J. K., and D. E. Hayes (1974), The Australian-Antarctic Discordance: New results and implications, *J. Geophys. Res.*, *79*, 2579–2587, doi:10.1029/JB079i017p02579.

Whittaker, J. M., R. D. Müller, and M. Gurnis (2010), Development of the Australian-Antarctic depth anomaly: Development of the AAD Anomaly, *Geochem. Geophys. Geosyst.*, *11*, Q11006, doi:10.1029/2010GC003276.